Journal of Colloid and Interface Science 333 (2009) 120–127

Contents lists available at ScienceDirect

Journal of Colloid and Interface Science

www.elsevier.com/locate/jcis

Zn_2Al layered double hydroxides intercalated and adsorbed with anionic blue dyes: A physico-chemical characterization

Rafael Marangoni [a], Mustapha Bouhent [b], Christine Taviot-Guého [c], Fernando Wypych [a,*], Fabrice Leroux [c,*]

[a] CEPESQ—Centro de Pesquisas em Química Aplicada, Departamento de Química, Universidade Federal do Paraná, UFPR, CP 19081, 81531-990, Curitiba, Paraná, Brazil
[b] Laboratoire de Physico-Chimie des Matériaux, Catalyse et Environnement, Université des Sciences et de la Technologie d'Oran, BP 1505 Oran El M'naouer, Algeria
[c] Laboratoire des Matériaux Inorganiques, UMR 6002, Université Blaise Pascal, 63177 Aubière Cedex, France

ARTICLE INFO

Article history:
Received 15 December 2008
Accepted 5 February 2009
Available online 10 February 2009

Keywords:
Layered double hydroxides
Dye
Intercalation
Adsorption
Thermodynamic constants

ABSTRACT

Three different anionic blue organic dyes have been intercalated into the structure of Zn_2Al layered double hydroxides, using the co-precipitation method at constant pH. Using the same synthetic procedure, Zn_2Al–Cl has been prepared and used as an adsorptive phase to retain the blue dyes from an aqueous solution. All the organic/inorganic (O/I) hybrid LDH compounds were analyzed by X-ray powder diffraction (XRPD), thermal analysis (TG/DTA), elemental analysis, solid state ^{13}C nuclear magnetic resonance (CPMAS ^{13}C NMR), and Fourier transform infrared spectroscopy (FTIR). In the adsorption experiments, Gibbs free energy ΔG values for the temperatures in a range between 10 and 40 °C were found to be negative, which indicates that the nature of adsorption is spontaneous and shows the affinity of LDH material towards the blue anionic dyes. Additionally a decrease in ΔG values at higher temperature further indicates that this process is even more favorable at these conditions. The enthalpy ΔH values were between physisorption and chemisorption, and it may be concluded that the process was a physical adsorption enhanced by a chemical effect, characterized by a combined adsorption/intercalation reaction, making these O/I assemblies reminiscent of the Maya blue.

1. Introduction

Hybrid organic/inorganic (O/I) assemblies constitute a suitable approach for obtaining multifunctional materials. More specifically, concerning the intercalation of dye organic molecules into inorganic hosts, the interest stems from the peculiar molecular arrangement imposed by the host structure, the thermal stability supplied by the inorganic constituent, and the stability against the dissolution process, the whole contributing to maintain the optical properties of the intercalated dye.

In the domain of hybrid dye inorganic assemblies, we must note the outstanding longevity of Maya blue which comes from a synergistic effect. Indeed, Maya blue arises from a very stable organo-clay complex formed of a superlattice of palygorskite matrix with indigo molecules and is resistant to dilute mineral acid and alkaline solutions, solvent treatment, moderate heat, and even biocorrosion. Another example is the beautiful Caribbean Sea blue color which remains unaltered after centuries of exposure under drastic conditions of temperature and humidity of the tropical forest [1–3]. Whether the indigo molecules seal the channels in palygorskite clay or penetrate into the structure channels [4,5] and whether iron is present as nanoparticles as amorphous goethite [6] or in substitution in the clay [7] still remain controversial topics.

In the 1990s, there was a strong interest in the dyes and their incorporation into inorganic host structures. This was exemplified by immobilizing compounds into zeolite open frameworks and intercalation into layered smectite-type 2:1 clay minerals, as shown in some reviews [8–11] and aromatic molecules such as substituted stilbene, naphthalene, and phenanthrene into zeolite [12,13] and clay minerals [14–16]. Even if most of the studies related to dyes and mineral clays are currently devoted to environmental purposes and more specifically to their sorption from aqueous solutions [17–22], a renewed interest for new types of application has recently emerged. Indeed, exceptional properties may be found from the synergism of the two counterparts that neither the clay nor the organic dye alone exhibit as beautifully illustrated by the Maya blue and, more recently, by synthetic hybrid materials which can find a place in laser applications [23] or for the replacement of environmentally toxic metal-based pigments in the paint and pigment industry [24].

Besides that and from the point of view of the organic molecule, the inorganic part acts to position and orientate structurally the guest species. Such sandwiched inorganic organic stacked structures have been mostly illustrated by cationic smect-

* Corresponding authors.
E-mail addresses: wypych@quimica.ufpr.br (F. Wypych), fabrice.leroux@univ-bpclermont.fr (F. Leroux).

0021-9797/$ – see front matter
doi:10.1016/j.jcis.2009.02.001

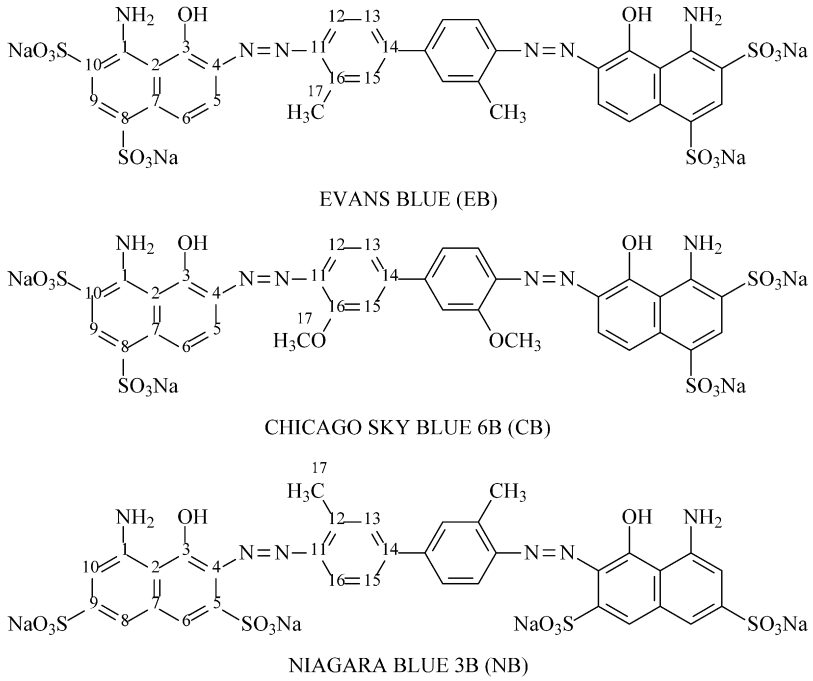

Fig. 1. Blue dyes molecular structures. Numbering of carbon atoms to attribution of ^{13}C nuclei NMR peaks.

ite-type mineral clays so far. Yet layered double hydroxides (LDH) and layered hydroxide salts (LHS) [25] also constitute two families of interest since they present a chemical versatility and a tunable layer charge density, ranging from 0.17 to 0.41 $C\,m^{-2}$ in layered double hydroxides [26]. The LDH structure refers to the natural hydrotalcite mineral, and this class of compounds is described with the ideal formula, $[M^{II}_{1-x}M^{III}_x(OH)_2]_{intra}[A^{m-}_{x/m}\cdot nH_2O]_{inter}$, where M^{II} and M^{III} are metal cations, A the anions, and *intra* and *inter* denote the intralayer and interlayer domains, respectively. The structure consists of brucite-like layers built up from edge-sharing $M(OH)_6$ octahedra. A partial and isostructural M^{II} to M^{III} substitution induces a positive charge for these layers, balanced with the presence of the hydrated interlayer anions. Owing to their high charge density, LDH materials are sometimes considered less than ideal hosts for many applications of porous pillared materials [27]; however, they should be able to strongly orientate the molecular arrangement within the interlayer space in a highly stowed fashion as the anions must satisfy and compensate the forming layer charge and therefore supply potentially strong intermolecular interactions. Conversely the inorganic LDH blocks may consider the organic component as a textural agent, thus orientating the textural properties of the whole as reported for the intercalation of large macromolecules such as polymers [28–31] and biomacromolecules such as DNA [32–34]. Some studies have reported on multibranched tetrafunctionalized porphyrin-type macromolecules [35,36] and perylene-type chromophores intercalated into hydrocalumite [37], as well as on the reversible color change of poly(diacetylenecarboxylates) incorporated into LDH [38], on the photo-sensitizing efficiency of intercalated 4-benzoyl benzoate for the oxidation of di-*n*-butylsulfide [39], or on the sunscreen effect of organic absorbents [40–42]. Some important findings were suggested by Costantino and co-workers on chromophores with donor acceptor properties [43], phenolphthalein [44], methyl orange [44,45], etc. Indeed, these authors have been pioneers in determining whether hydrotalcite-type materials were able to intercalate large size dye and in obtaining information on the orientation/conformation of the dye by basal spacing measurements and photophysical properties [45,46]. They also observed shifts in the absorption spectra associated with intermolecular interactions; yet, co-intercalation often occurred and ill-defined assemblies were obtained from the incorporation of large dye molecules [47,48].

Having successfully prepared polymer LDH assemblies by the so-called coprecipitation method [26], we have developed here a similar approach to incorporate three cumbersome commercially blue anionic dyes, Evans blue (EB), Chicago blue sky (CB), and Niagara blue (NB) presenting quite similar molecular structures, into Zn/Al layered double hydroxides. The process of immobilization was studied by direct coprecipitation synthesis and adsorption properties onto Zn_2Al–Cl LDH were also examined. In the adsorption/intercalation experiments, thermodynamic data were obtained and attributed to adsorption/intercalation reactions.

2. Materials and methods

Dye sodium salts, Evans blue ($C_{34}H_{24}O_{14}N_6S_4Na_4$, direct blue 53, Aldrich, 40%) noted as EB, Chicago sky blue 6B ($C_{34}H_{24}O_{16}N_6S_4Na_4$, Aldrich 65%) noted as CB, Niagara blue 3B ($C_{34}H_{24}O_{14}N_6S_4Na_4$, Aldrich, 30%) noted as NB, and $ZnCl_2\cdot 5H_2O$ (Acros), $Al(NO_3)_3\cdot 9H_2O$ (Acros, 99%), and NaOH (Acros, >97%) were used. The molecular structures of the used dyes are shown in Fig. 1.

The syntheses of the Zn/Al–dye LDH were carried out using the well-known coprecipitation method and previously described [49] and briefly reproduced below. The amount of dye molecule was optimized to 4 times the content of Al^{3+} cations, defined as the anionic exchange capacity of the LDH material. Typically, 10^{-2} mol of dye was dissolved into 500 ml of a solution of decarbonated water. To this solution, two other solutions were added dropwise, one containing 5×10^{-3} mol of $ZnCl_2\cdot 5H_2O$ and 2.5×10^{-3} mol of $AlCl_3\cdot 6H_2O$, and the other NaOH, 1 mol/L. The addition was performed at constant pH of 9, under nitrogen atmosphere and vigorous stirring, and completed after 24 h. The precipitate was aged in the mother liquid for an additional period of time of 24 h under nitrogen atmosphere to avoid the contamination by carbonate, from the atmospheric CO_2. The product was centrifuged and then washed five times with decarbonated water and dried at room temperature. The intercalation compounds are denoted as Zn_2Al–dye, where dye is the respective dye utilized in the synthesis.

Zn_2Al–Cl LDH was also synthesized using the same proportion of Zn and Al, in the same way as for Zn/Al–dye.

Elemental analysis (H, S, Zn, and Al) was performed at the Vernaison Analysis Center of CNRS using inductive conduction plasma coupled to atomic emission spectroscopy (ICP/AES). The water molecule content was calculated from the weight loss at 200 °C under air expressed by $(OH)_2$ as $Zn_aAl_b(OH)_2(dye)_c{\cdot}nH_2O$, where a, b, and c were calculated from the chemical analyses and the number of water molecule n was given by TG analysis.

For the X-ray powder diffraction (XRPD) measurements, a Philips X-Pert Pro diffractometer was used, which was equipped with a Cu X-ray tube, graphite monochromator, and Ar-filled proportional counter. Divergence and receiving slits were 1/16° and 1 mm, respectively. Powders were backloaded in an aluminum sample holder to produce a good sample surface and to avoid preferential orientation effects. Data were collected in a step scan mode between 2.0° and 90° (2θ) with a step size of 0.03° and a counting time of 10–20 s/step, depending on the crystallinity.

The FTIR spectra were collected in a Bomem Michelson MB100 spectrometer. Tablets of KBr were prepared after mixing 1% of the sample with dry KBr and pressed to 8 tons, being the analyses performed by transmission mode, in the range from 4000 to 400 cm^{-1}, with a resolution of 2 cm^{-1} and accumulation of 32 scans.

^{13}C (I = 1/2) solid state NMR experiments were performed with a 300 Bruker spectrometer at 75.47 MHz. The experiments were carried out using magic angle spinning (MAS) conditions at 10 kHz and a 4 mm diameter size zirconia rotor. ^{13}C spectra obtained by the proton-enhanced cross-polarization method (CP) are referenced to the carbonyl group of glycine, calibrated at 176.03 ppm. The CP conditions were as follows: ^1H (90°) pulse width of 3.5 µs, contact time of 1 ms, ^1H decoupling during acquisition (AQ = 29.33 ms), and recycling time of 3 s. For the hybrid materials, 10,000 scans were needed to obtain a proper signal to noise ratio.

The adsorption isotherms were carried out by the batch equilibration technique. Fifty milligrams of the Zn_2Al/Cl layered double hydroxide was dispersed in 50 ml of deionized and decarbonated water. Dye solutions were prepared in an appropriate range of concentrations to obtain a final volume of 50 ml after the addition of the inorganic sample and the pH was fixed at 7. The batch reactors were kept at constant temperature of 10, 25, or 40 °C in a thermostatic container. An UV–visible spectrometer, Lambda 2S Perkin–Elmer, was used to measure the absorbance at specific wavelengths according to the nature of the dye (608 nm for EB, 620 nm for CB, and 594 nm for NB). The amount of organic adsorbed by the LDH (q_e) was determined from the difference between the initial (C_i, batch dye concentration) and the final concentration (C_e, adsorbate concentration at equilibrium after a contact time of 24 h) per gram of adsorbent according to the relation: $q_e = (C_i - C_e) \times V/m$, where V and m are the total volume and the adsorbate mass, respectively. The adsorption isotherms were obtained by plotting (q_e) vs (C_e).

The thermal analysis measurements (TG/DTA) were obtained in a Mettler Toledo TGA/s-DTA851e equipment, using platinum crucibles, flow of oxygen (50 ml min^{-1}), and heating rate of 10° min^{-1}.

3. Results and discussion

The elemental analysis gave the results (expressed in percentage). For Zn_2Al–EB, Zn = 26.62, Al = 5.66, S = 6.45; for Zn_2Al–CB, Zn = 21.79, Al = 4.71, S = 5.26; and for Zn_2Al–NB, Zn = 25.74, Al = 5.31, and S = 5.89. Using the elemental analysis and the water content obtained by TG analysis, the chemical compositions were determined as follows: Zn_2Al–EB = $Zn_{0.66}Al_{0.34}(OH)_2(EB)_{0.082}(CO_3)_{0.006}{\cdot}0.49H_2O$; Zn_2Al–CB = $Zn_{0.65}Al_{0.34}(OH)_2(CB)_{0.080}(CO_3)_{0.01}{\cdot}0.81H_2O$, and Zn_2Al–NB = $Zn_{0.66}Al_{0.33}(OH)_2(NB)_{0.079}(CO_3)_{0.007}{\cdot}0.65H_2O$, where the amount of the tetranegative anionic dye in each compounds is very close to the theoretical value of 0.085 for EB and CB and 0.0825 for NB. It can be observed that in all compounds the Zn/Al ratio of 2 is obtained and that only traces of carbonate are necessary for the formula charge balance. Taking into account the formula of $Zn_{0.66}Al_{0.34}(OH)_2(EB)_{0.082}(CO_3)_{0.006}{\cdot}(H_2O)_{0.49}$ and $Zn_{0.66}Al_{0.34}(OH)_2Cl_{0.34}{\cdot}0.67H_2O$ (phase used in the adsorption experiments), the anionic exchange capacities (AEC) are 195 and 308 meq/100 g, respectively.

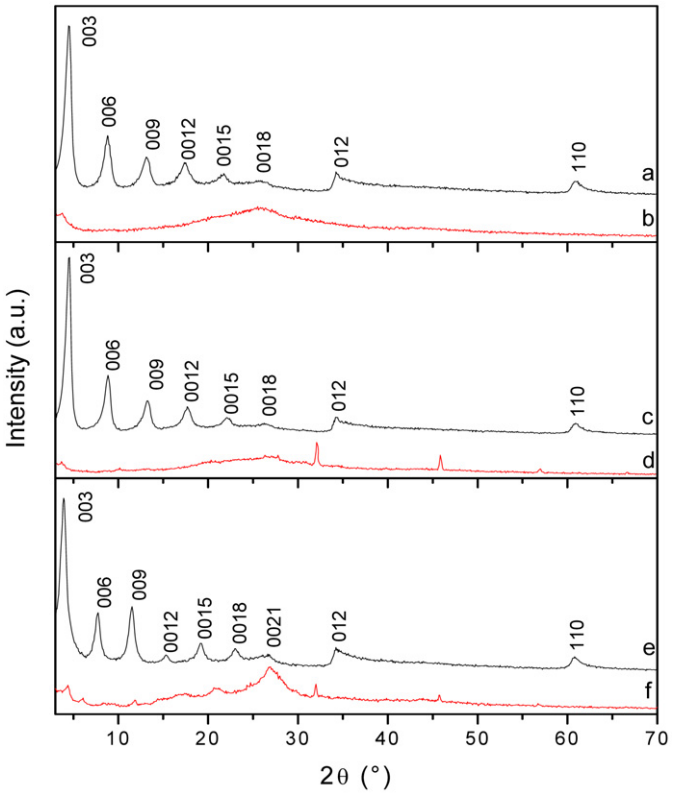

Fig. 2. X-ray diffraction pattern of Zn_2Al–EB (a), pure EB (b), Zn_2Al–CB (c), pure CB (d), Zn_2Al–NB (e), pure NB (f).

XRPD patterns of Zn_2Al–EB, Zn_2Al–CB, and Zn_2Al–NB and their respectively pristine dyes are shown in Fig. 2.

From the XRPD patterns, all the intercalation compounds appear as well crystallized and a large number of basal peaks, indicating the presence of an ordered stacking sequence. The observed basal distance was of 20.6 Å for Zn_2Al–EB, 20.4 Å for Zn_2Al–CB, and 23.4 Å for Zn_2Al–NB, respectively. The different basal distances are explained by the fact that both EB and CB have functionalized groups located at the same positions, and a herringbone-type accommodation is then observed for these interleaved molecules, whereas for NB the functionalized groups are disposed on a same side of the molecule. A gap in the electronic density along the stacking sequence suggests that NB is disposed in double layer arrangement within LDH interlayer space, as previously reported [49].

In comparison with the XRPD patterns of the pure dyes, it was observed that the obtained intercalation compounds were not contaminated neither with the dye used in the synthesis nor with carbonate and/or chloride. Our results are in agreement with a previous study reporting the incorporation of EB within LDH interlayer space [50], but the LDH compound was very ill defined in the later case, showing low crystallinity and small crystal sizes.

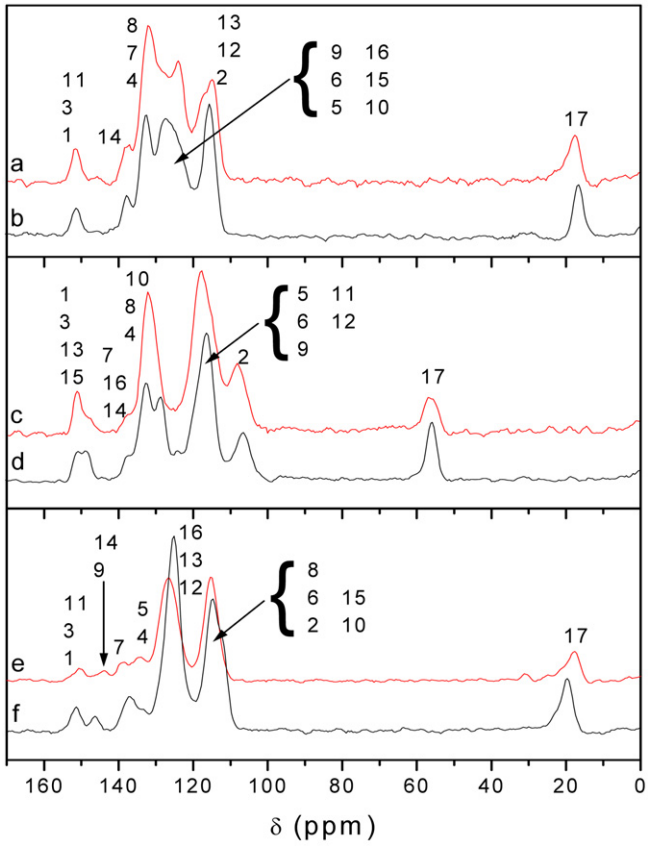

Fig. 3. ^{13}C CPMAS NMR spectra: pure EB (a), Zn_2Al–EB (b), pure CB (c), Zn_2Al–CB (d), pure NB (e), Zn_2Al–NB (f).

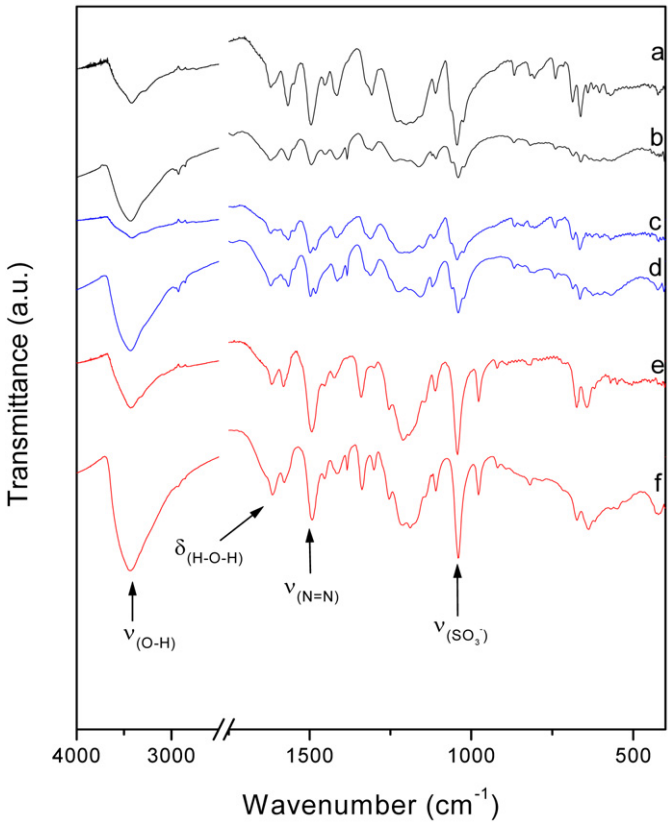

Fig. 4. FTIR spectra: pure EB (a), Zn_2Al–EB (b), pure CB (c), Zn_2Al–CB (d), pure NB (e), Zn_2Al–NB (f).

The arrangement of the dye molecules was already described in a previous publication [49].

Solid state NMR ^{13}C CP-MAS spectra of the dye molecules and their hybrid LDH derivatives are displayed in Fig. 3 and the numbering of carbon atoms is displayed in Fig. 1.

Organic blue molecules present a naphthalene cycle on which the four sulfonate groups are linked, C(8) and C(10) for CB and EB, and C(5) and C(9) for EB, and with amino and hydroxyl groups on C(1) and C(3), respectively. We were interested in observing the effect of the layer entrapment on the NMR spectra. However due to the strong overlapping in the resonance lines, it is difficult to scrutinize such an effect, and the assignment of the carbon nuclei atom is reported in the figure for guideline only. Nevertheless, it can be observed that the spectra of CB and EB dye molecules superimpose quite well with their corresponding hybrid phases. It means that in both cases the dye anion is keeping its chemical integrity and that the electrostatic attraction between them and the inner surface of LDH host material is not sufficient enough to change the carbon atom local environment. Interestingly, the spectrum is slightly different between the NB and its LDH-related intercalated phase. A down-field shift is observed for C(5) and C(9), directly connected to the sulfonate groups, and a same shift is observed for the methylene group C(17), while all the other carbon nuclei remain at a similar chemical shift. These perceptible shifts may be related to some much stronger interaction between NB and LDH layers.

The FTIR spectra of the Zn/Al–dye LDH are shown in Fig. 4, which are dominated by the vibration peaks of the dyes.

The strong and broad absorption band observed around 3434 cm^{-1} corresponds to the O–H stretching vibration of the layer surface and/or interlayer water molecules and the band in 1625 cm^{-1} is due to O–H bending vibration of water molecules. The lower values of O–H stretching vibration in comparison with the free OH groups (>3650 cm^{-1}) indicate that the OH groups are involved in hydrogen bonding with the dyes. The bands observed in the low-frequency region of the spectrum (<600 cm^{-1}) can be interpreted as the lattice vibration modes, such as the M–O–H vibration and O–M–O stretching. In the I/O hybrids, the symmetric sulfonate vibration peak at 1040 cm^{-1} shows a slight shift to lower frequency regions, when compared with those of the pure dye salts, the same occurs to the asymmetric sulfonate vibration around 1170 cm^{-1}. This fact indicates that the interactions between the intercalated dye anions and the hydroxide layers are different from those in the dye salts. The characteristic vibration band of azo groups appears around 1492 cm^{-1}. The remaining peaks are due to the stretching and bending vibrations of the aromatic rings framework. The similarity of spectra in the range between 1750 and 500 cm^{-1}, in comparison with the Zn/Al–dye LDH and the respective pure dyes, indicates that the molecular structures of the blue dyes anions are similar in both situations.

The TG/DTA analysis for the Zn_2Al–dye and the pure dyes is shown in Fig. 5. The three intercalated compounds exhibit a thermal behavior that is composed by a dehydration of the compound by loss of water adsorbed and intercalated into the LDH (endothermic event), followed by a second endothermic event due to dehydroxylation of the LDH matrix and exothermic events due to burning of the organic dyes.

For the Zn_2Al–NB, it was observed in the DTA curve an endothermic peak centered at 114 °C due to loss of water molecules and its represents a loss of mass of 16.2% in the TG curve, a small endothermic peak at 263 °C due to matrix dehydroxylation, and at 560 and 610 °C appears two exothermic peaks that correspond to a loss of mass of 27.4% due to the burning of the intercalated anionic dyes. The Zn_2Al–CSB shows a endothermic peak at 100 °C relative to the loss of water (13.1% loss mass), the dehydroxylation process appears at 244 °C, and a large exothermic peak centered at

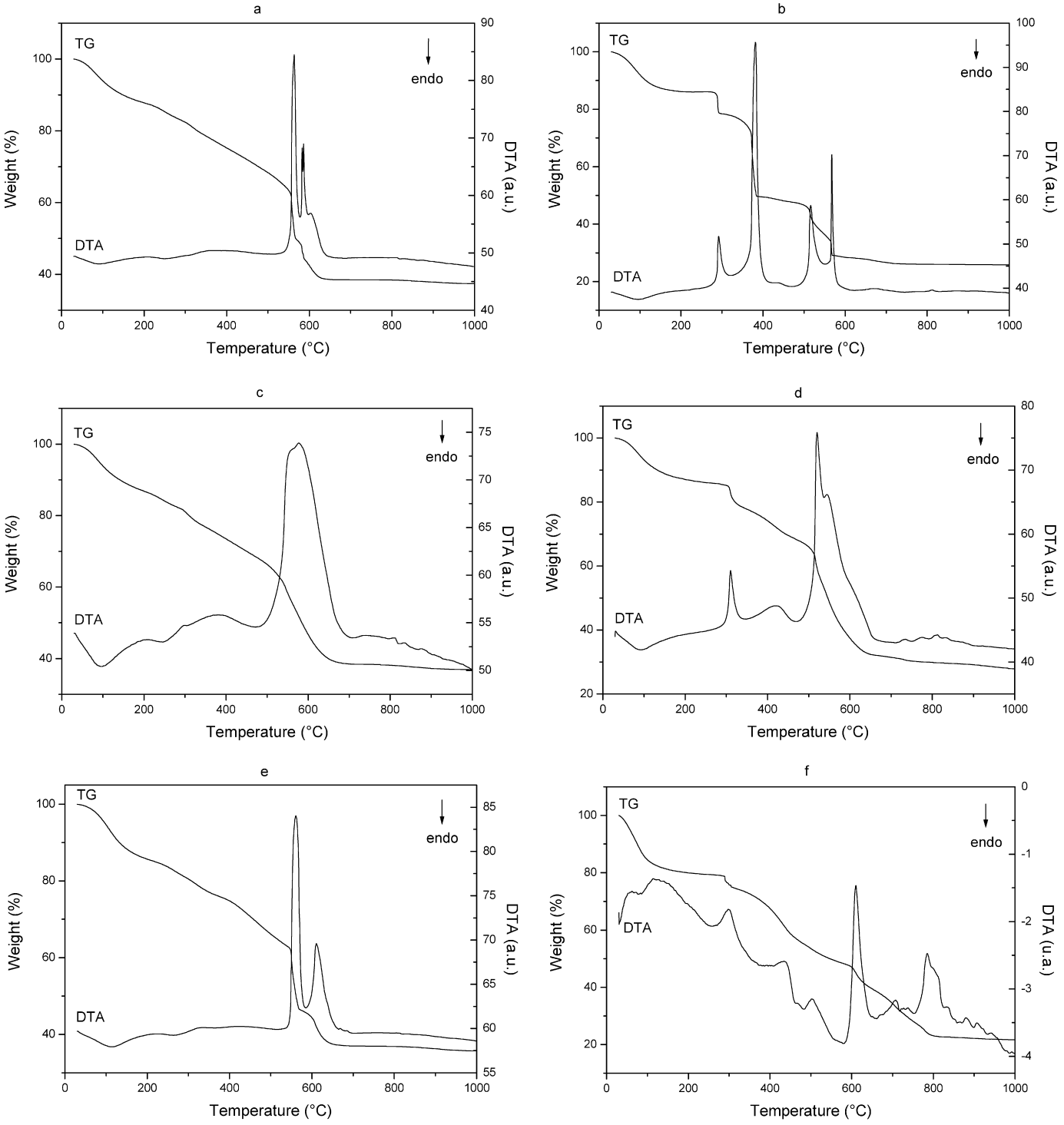

Fig. 5. TG/DTA curves of the Zn_2Al–EB (a), EB (b), Zn_2Al–CSB (c), CSB (d), Zn_2Al–NB (e), NB (f).

575 °C relative to the oxidation of the dye (29.9% loss of mass). In the Zn_2Al/EB, endothermic peaks at 91 °C (12.5%) and 249 °C were observed, which can be attributed to the loss of water and to a dehydroxylation process, respectively. It was observed also exothermic peaks at 561 and 584 °C and a small peak at 602 °C due to loss of mass related to the desorption and breakdown of the dye as well as probable evolution of NO_x and SO_x.

After the intercalation process, it was possible to observe an increase in the thermal stability of the dyes. Indeed the comparison of TG/DTA curves between the pure dyes and their intercalated derivative phases let us observe that the dye decomposition event observed around 300 °C is largely shifted to 470 °C and up to 530 °C.

Fig. 6 shows the adsorption isotherms of the blue dyes onto a LDH Zn_2Al–Cl phase for each blue dye at three different investigated temperatures.

The adsorption data are usually presented as adsorption isotherm at constant temperature and the interpretations may use several adsorption equilibrium models to describe the liquid/solid interface phase, such as the Langmuir, Freundlich, and Redlich–Peterson [17,51]. The Langmuir model is the most used and common model to describe the adsorption properties. This model sup-

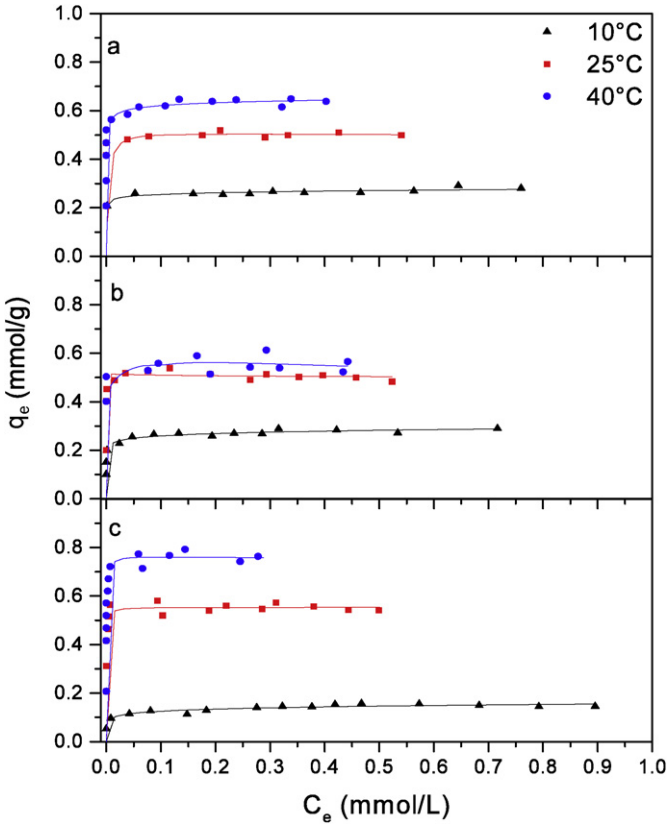

Fig. 6. Adsorption isotherms for Evans blue (a), Chicago sky blue 6b (b), and Niagara blue 3b (c), onto Zn_2Al–Cl phase.

poses that the adsorption sites are homogeneous and each site is accommodating one molecule only. Moreover the adsorption occurs in a monolayer form and there is no interaction between adsorbed molecules. The Langmuir isotherm is represented by

$$q_e = \frac{q_m K_L C_e}{1 + K_L C_e}. \tag{1}$$

Its linear expression can be written as

$$\frac{C_e}{q_e} = \frac{1}{q_m K_L} + \frac{C_e}{q_m}, \tag{2}$$

where q_e is the amount of dye adsorbed per unit mass of adsorbent (mg/g), C_e is the equilibrium dye concentration (mg/L) and q_m and K_L are the Langmuir constants representing the monolayer adsorption capacity (mg/g) and the energy of adsorption (L/mg), respectively. The plot of C_e/q_e versus C_e gives a straight line with a slope of $1/q_m$ and an intercept of $1/q_m K_L$, from which q_m and K_L can be obtained. Table 1 shows the Langmuir constants for the blues adsorbed in the Zn_2Al–Cl phase.

The adsorption isotherm constants obtained were used to calculate the thermodynamic parameters such as Gibbs free energy, enthalpy, and entropy. The equilibrium experiments performed at three temperatures showed an increase in the amount of dye adsorbed, implying an endothermic nature of the adsorption process. The Gibbs free energy change (ΔG) is the basic criterion of spontaneity and a negative value indicates that the reaction is spontaneous. By using the equilibrium constant K_L obtained for each temperature from the Langmuir model, ΔG can be calculated by using Eq. (3) and the enthalpy and entropy change (ΔH and ΔS, respectively) can be determined by using Eqs. (4) and (5),

$$\Delta G = -RT \ln K_L, \tag{3}$$

$$\Delta G = \Delta H - T\Delta S, \tag{4}$$

Table 1
Langmuir constants for the blue molecules adsorbed onto Zn_2Al–Cl phase.

	T (°C)	q_m (mmol/g)	K_L (L/mmol)	R^2
EB	10	0.284	59.924	0.9956
	25	0.512	1025.774	0.9992
	40	0.638	1393.689	0.9992
CB	10	0.285	155.601	0.9976
	25	0.505	784.456	0.9955
	40	0.535	1082.639	0.9987
NB	10	0.151	80.564	0.9954
	25	0.558	1253.894	0.9990
	40	0.778	1647.270	0.9985

Table 2
Thermodynamic data for the blues adsorbed on the Zn_2Al–Cl phase.

	T (°C)	ΔG (kJ/mol)	ΔH (kJ/mol)	ΔS (J/K mol)
EB	10	−9.64	78.31	313.70
	25	−17.19		
	40	−18.88		
CB	10	−11.88	48.16	213.64
	25	−16.52		
	40	−18.19		
NB	10	−10.33	75.12	304.83
	25	−17.68		
	40	−19.29		

$$\ln K_L = -\frac{\Delta G}{RT} = -\frac{\Delta H}{RT} + \frac{\Delta S}{R}, \tag{5}$$

where T is the temperature (K), R the universal gas constant (8.314 J mol^{-1} K^{-1}), and K_L the Langmuir constant. The van't Hoff plot of $\ln K_L$ as a function of $1/T$ (figure not shown) yielded a straight line from which ΔH and ΔS were calculated from the slope and intercept, respectively (see Table 2). The change of free energy for physisorption is usually between −20 and 0 kJ/mol, whereas chemisorptions are in the range of −80 to 400 kJ mol^{-1} [52]. The ΔG values for the used temperatures are negative, which indicate that the nature of adsorption is spontaneous and that the affinity of LDH material toward the blue organic dyes is strong. More negative values of ΔG at higher temperatures show that the process is more favorable under these conditions. The ΔH values are in the middle of physisorption and chemisorption, and it may be concluded that the process was a physical adsorption enhanced by a chemical effect (intercalation reaction). The positive value of ΔH indicates that the adsorption is endothermic and further suggests that adsorption is a physisorption involving weak forces of attraction. The positive value of ΔS indicates a rather good affinity of the material with dye molecules and is a sign of an increase in the degree of freedom of the adsorbed species [17,51,52].

The phases isolated after the adsorption experiments were systematically submitted to X-ray diffraction studies. As can be seen in Fig. 7, the partial replacement of chloride ions by the anionic dye is occurring concomitantly with the adsorption process.

By analysing the powder diffraction patterns series for each dye, the intercalation process is found to be more pronounced for the EB since the dye anions are intercalated into the interlayer domain, while for CB and NB, a partial intercalaltion was observed only. In the case of EB series, based on the calculated intercalation indices, the amount of retained dye is attributed mainly to an intercalation reaction, especially in high concentration solutions. Indeed the intercalation process confirms the values of ΔH near to chemisorption values and further indicates that the adsorption process is of mixed physical and chemical nature. This fact can

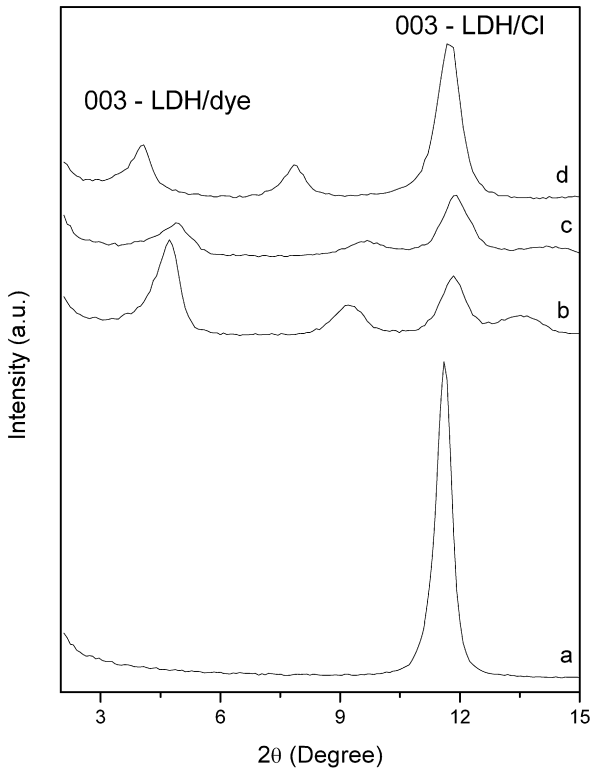

Fig. 7. X-ray diffractions patterns of the compounds obtained after the adsorption studies at 25 °C and 1 g/L of concentration: Zn_2Al–Cl (a), EB adsorbed/intercalated (b), CB adsorbed/intercalated (c), and NB adsorbed/intercalated (d).

indicate that the Langmuir isotherm does not make a distinction among the external adsorption sites and the interlayer sites of LDH. Some recent works have also demonstrated that such phenomena, intercalation, and adsorption processes may also occur in different other matrices [53–57].

4. Summary

As demonstrated by XRPD characterization, the intercalation of dye molecules into LDH lattices yields to an ordered molecular arrangement. It is noteworthy that after either adsorption and/or intercalation, the interfacial interaction between the blue molecule and the LDH material preserves them from dissolution. Therefore the observed increase of the thermal stability combined with the stabilization against dissolution makes these organic/inorganic assemblies reminiscent of the Maya blue and of the Bauer et al. study [37].

The adsorption studies have shown that the adsorption process does not occur on the surface of the LDH only but an intercalation process is also occurring concomitantly according to the thermodynamical values, which were found to be in agreement with the XRPD characterizations. We believe that such intercalated/adsorbed organic/inorganic and stabilized materials may be potentially interesting as colored filler for polymer and cements as pointed out recently [36,49,56].

Acknowledgments

The authors acknowledge FINEP, CNPq, Brazilian financial agencies, and Dr. José Eduardo Ferreira da Costa Gardolinski for performing the TG/DTA measurements. R.M. thanks also CAPES for funding permitting his stay at LMI and M.B. thanks funding project PHC Tassili 06MDU676.

References

[1] R.J. Gettens, Am. Antiquity 27 (1962) 557.
[2] H. Van Olphen, Science 154 (1966) 645.
[3] M.J. Yacamán, L. Rendón, J. Arenas, M.C. Serra Puche, Science 273 (1996) 223.
[4] B. Hubbard, W. Kuang, A. Moser, G.A. Facey, C. Detellier, Clays Clay Miner. 51 (2003) 318.
[5] E. Fois, A. Gamba, A. Tilocca, Microporous Mesoporous Mater. 57 (2003) 263.
[6] L.A. Polette, G. Meitzner, M.J. Yacaman, R.R. Chianelli, Microchem. J. 71 (2002) 167.
[7] M. Sanchez del Rio, A. Sodo, S.G. Eeckhout, T. Neisius, P. Martinetto, E. Dooryhée, C. Reyes-Valerio, Nucl. Instrum. Methods Phys. B 238 (2005) 50.
[8] M. Ogawa, K. Kuroda, Chem. Rev. 95 (1995) 399.
[9] G. Schulz-Ekloff, D. Wöhrle, B. van Duffel, R.A. Schoonheydt, Microporous Mesoporous Mater. 51 (2002) 91.
[10] D. Wöhrle, G. Schlz-Ekloff, Adv. Mater. 6 (1994) 875.
[11] G. van der Goor, K. Hoffmann, S. Kallus, F. Marlow, F. Schüth, P. Behrens, Adv. Mater. 8 (1996) 65.
[12] V.J. Ramamurthy, Am. Chem. Soc. 116 (1994) 1345.
[13] V. Ramamurthy, D.F. Eaton, Chem. Mater. 6 (1994) 1128.
[14] R.A. Schoonheydt, L. Heughebaert, Clay Miner. 27 (1992) 91.
[15] R.A. Schoonheydt, P. Pauw, D. Vliers, F.C. Schriver, J. Phys. Chem. 88 (1984) 5113.
[16] G. Villemure, C. Detellier, A.G. Szabo, J. Am. Chem. Soc. 108 (1986) 4658.
[17] M.-X. Zhu, Y.-P. Li, M. Xie, H.-Z. Xin, J. Hazard. Mater. B 120 (2005) 163.
[18] Z. Bouberka, S. Kacha, M. Kameche, S. Elmaleh, Z. Derriche, J. Hazard. Mater. B 119 (2005) 117.
[19] M.-Y. Chang, R.-S. Juang, J. Colloid Interface Sci. 278 (2004) 18.
[20] J. Orthman, H.Y. Zhu, G.Q. Lu, Sep. Purif. Technol. 31 (2005) 53.
[21] Z. Sun, Y. Chen, Q. Ke, Y. Yang, J. Yuan, J. Photochem. Photobiol. A 149 (2002) 169.
[22] R. Kun, M. Balázs, I. Dékány, Colloids Surf. A 265 (2005) 155.
[23] G. Ihlein, F. Schüth, O. Krau, U. Vietze, F. Laeri, Adv. Mater. 10 (1998) 1117.
[24] M. Ganschow, M. Wark, D. Wöhrle, G. Schilz-Ekloff, Angew. Chem. 112 (2000) 167.
[25] G.G.C. Arizaga, K.G. Satyanarayana, F. Wypych, Solid State Ionics 178 (2007) 1143.
[26] F. Leroux, C. Taviot-Guého, J. Mater. Chem. 15 (2005) 3628.
[27] H. Hata, Y. Kobayashi, T.E. Mallouk, Chem. Mater. 19 (2007) 79.
[28] C.O. Oriakhi, I.V. Farr, M.M. Lerner, J. Mater. Chem. 6 (1996) 103.
[29] G.A. Bubniak, W.H. Schreiner, N. Mattoso, F. Wypych, Langmuir 18 (2002) 5967.
[30] F. Leroux, J.-P. Besse, Chem. Mater. 13 (2001) 3507.
[31] M. El Moujahid, J.-P. Besse, F. Leroux, J. Mater. Chem. 12 (2002) 3324.
[32] J.H. Choy, S.Y. Kwak, J.S. Park, Y.J. Jeong, J. Portier, J. Am. Chem. Soc. 121 (1999) 1399.
[33] J.H. Choy, S.Y. Kwak, J.S. Park, Y.J. Jeong, J. Mater. Chem. 11 (2001) 1671.
[34] L. Désigaux, M.B. Belkacem, J. Cellier, P. Léone, L. Cario, F. Leroux, C. Taviot-Guého, B. Pitard, Nano Lett. 2 (2006) 199.
[35] M. Halma, K.A.D.F. Castro, C. Taviot-Gueho, V. Prevot, C. Forano, F. Wypych, S. Nakagaki, J. Catal. 257 (2008) 233.
[36] H. Tagaya, A. Ogata, T. Kuwahara, S. Ogata, M. Karasu, J.-I. Kadokawa, K. Chiba, Microporous Mater. 7 (1996) 151.
[37] J. Bauer, P. Behrens, M. Speckbacher, H. Langhals, Adv. Funct. Mater. 13 (2003) 241.
[38] T. Itoh, T. Shichi, T. Yui, H. Takahashi, Y. Inui, K. Takagi, J. Phys. Chem. B 109 (2005) 3199.
[39] T. Pigot, J.C. Dupin, H. Martinez, C. Cantau, M. Simon, S. Lacombe, Microporous Mesoporous Mater. 84 (2005) 343.
[40] A.M. El-Toni, S. Yin, T. Sato, J. Solid State Chem. 177 (2004) 3197.
[41] A.M. El-Toni, S. Yin, T. Sato, Mater. Chem. Phys. 89 (2005) 154.
[42] Q. He, S. Yin, T. Sato, J. Phys. Chem. Solids 65 (2004) 395.
[43] G.G. Aloisi, U. Costantino, F. Elisei, L. Latterini, C. Natali, M. Nocchetti, J. Mater. Chem. 12 (2002) 3316.
[44] L. Latterini, F. Elisei, G.G. Aloisi, U. Costantino, M. Nocchetti, Phys. Chem. Chem. Phys. 4 (2002) 2792.
[45] U. Costantino, N. Coletti, M. Nocchetti, G.G. Aloisi, F. Elisei, Langmuir 15 (1999) 4454.
[46] U. Costantino, N. Coletti, M. Nocchetti, G.G. Aloisi, F. Elisei, L. Latterini, Langmuir 16 (2000) 10351.
[47] L. Latterini, M. Nocchetti, G.G. Aloisi, U. Costantino, F. Elisei, Inorg. Chim. Acta 360 (2007) 728.
[48] M.Z. Bin Hussein, Z. Zainal, A.H. Yahaya, A.B.A. Aziz, Mater. Sci. Eng. B 88 (2002) 98.
[49] R. Marangoni, C. Taviot-Guého, A. Illaik, F. Wypych, F. Leroux, J. Colloid Interface Sci. 326 (2008) 366.
[50] M.Z. Bin Hussein, A.H. Yahaya, L.M. Ping, Dyes Pigm. 63 (2004) 135.
[51] Q. Hu, Z. Xu, S. Qiao, F. Haghseresht, M. Wilson, G.Q. Lu, J. Colloid Interface Sci. 308 (2007) 191.
[52] F. Renault, N. Morin-Crini, F. Gimbert, P. Badot, G. Crini, Bioresour. Technol. 99 (2008) 7573.

[53] M. Roulia, A.A. Vassiliadis, Microporous Mesoporous Mater. 116 (2008) 732.
[54] L. El Gaini, M. Ladraimi, E. Sebbar, A. Meghea, M. Bakasse, J. Hazard. Mater. 161 (2009) 627.
[55] G. Bascialla, A.E. Regazzoni, Colloids Surf. A 328 (2008) 34.
[56] C. Taviot-Guého, A. Illaik, C. Vuillermoz, S. Commereuc, V. Verney, F. Leroux, J. Phys. Chem. Solids 68 (2007) 1140.
[57] S.J. Palmer, A. Soisonard, R.L. Frost, J. Colloid Interface Sci. 329 (2009) 404.